Differential Branching Fraction and Angular Analysis of the Decay $B^0 \to K^{*0}\mu^+\mu^-$

R. Aaij *et al.**
(LHCb Collaboration)

(Received 15 December 2011; published 3 May 2012)

The angular distributions and the partial branching fraction of the decay $B^0 \to K^{*0}\mu^+\mu^-$ are studied by using an integrated luminosity of 0.37 fb^{-1} of data collected with the LHCb detector. The forward-backward asymmetry of the muons, $A_{\rm FB}$, the fraction of longitudinal polarization, $F_{\rm L}$, and the partial branching fraction $d\mathcal{B}/dq^2$ are determined as a function of the dimuon invariant mass. The measurements are in good agreement with the standard model predictions and are the most precise to date. In the dimuon invariant mass squared range 1.00–6.00 GeV$^2/c^4$, the results are $A_{\rm FB} = -0.06^{+0.13}_{-0.14} \pm 0.04$, $F_{\rm L} = 0.55 \pm 0.10 \pm 0.03$, and $d\mathcal{B}/dq^2 = (0.42 \pm 0.06 \pm 0.03) \times 10^{-7}\ c^4/\text{GeV}^2$. In each case, the first error is statistical and the second systematic.

DOI: 10.1103/PhysRevLett.108.181806 PACS numbers: 13.20.He

The process $B^0 \to K^{*0}\mu^+\mu^-$ is a flavor changing neutral current decay. In the standard model (SM) such decays are suppressed, as they can proceed only via loop processes involving electroweak penguin or box diagrams. As-yet undiscovered particles could give additional contributions with comparable amplitudes, and the decay is therefore a sensitive probe of new phenomena. A number of angular observables in $B^0 \to K^{*0}\mu^+\mu^-$ decays can be theoretically predicted with good control of the relevant form factor uncertainties. These include the forward-backward asymmetry of the muons, $A_{\rm FB}$, and the fraction of longitudinal polarization, $F_{\rm L}$, as functions of the dimuon invariant mass squared, q^2 [1]. These observables have previously been measured by the *BABAR*, Belle, and CDF experiments [2]. A more precise determination of $A_{\rm FB}$ is of particular interest as, in the $1.00 < q^2 < 6.00$ GeV$^2/c^4$ region, previous measurements favor an asymmetry with the opposite sign to that expected in the SM. If confirmed, this would be an unequivocal sign of phenomena not described by the SM. This Letter presents the most precise measurements of $A_{\rm FB}$, $F_{\rm L}$, and the partial branching fraction $d\mathcal{B}/dq^2$ to date. The data used for this analysis were taken with the LHCb detector at CERN during 2011 and correspond to an integrated luminosity of 0.37 fb^{-1}. The K^{*0} is reconstructed through its decay into the $K^+\pi^-$ final state.

The LHCb detector [3] is a single-arm spectrometer designed to study b-hadron decays. A silicon strip vertex detector positioned around the interaction region is used to measure the trajectory of charged particles and allows the reconstruction of the primary proton-proton interactions and the displaced secondary vertices characteristic of B-meson decays. A dipole magnetic field and further charged particle tracking stations allow momenta in the range $5 < p < 100$ GeV$/c$ to be determined with a precision of $\delta p/p = 0.4\%$–0.6%. The experiment has an acceptance for charged particles with pseudorapidity between 2 and 5. Two ring imaging Cherenkov detectors allow kaons to be separated from pions or muons over a momentum range $2 < p < 100$ GeV$/c$. Muons are identified on the basis of the number of hits in detectors interleaved with an iron muon filter.

The $B^0 \to K^{*0}\mu^+\mu^-$ angular distribution is governed by six q^2-dependent transversity amplitudes. The decay can be described by q^2 and the three angles θ_l, θ_K, and ϕ. For the B^0 ($\bar{B}^0$), θ_l is the angle between the μ^+ (μ^-) and the opposite of the B^0 ($\bar{B}^0$) direction in the dimuon rest frame, θ_K the angle between the kaon and the direction opposite to the B meson in the K^{*0} rest frame, and ϕ the angle between the $\mu^+\mu^-$ and $K^+\pi^-$ decay planes in the B rest frame. The inclusion of charge conjugate modes is implied throughout this Letter. At a given q^2, neglecting the muon mass, the normalized partial differential width integrated over θ_K and ϕ is

$$\frac{1}{\Gamma}\frac{d^2\Gamma}{d\cos\theta_l dq^2} = \frac{3}{4}F_{\rm L}(1-\cos^2\theta_l) + \frac{3}{8}(1-F_{\rm L})(1+\cos^2\theta_l) + A_{\rm FB}\cos\theta_l, \tag{1}$$

and integrated over θ_l and ϕ it is

$$\frac{1}{\Gamma}\frac{d^2\Gamma}{d\cos\theta_K dq^2} = \frac{3}{2}F_{\rm L}\cos^2\theta_K + \frac{3}{4}(1-F_{\rm L})(1-\cos^2\theta_K). \tag{2}$$

These expressions do not include any broad S-wave contribution to the $B^0 \to K^+\pi^-\mu^+\mu^-$ decay and any

*Full author list given at the end of the article.

contribution from low mass tails of higher K^{*0} resonances. These contributions are assumed to be small and are neglected in the rest of the analysis.

Signal candidates are isolated from the background by using a set of selection criteria which are detailed below. An event-by-event weight is then used to correct for the bias induced by the reconstruction, trigger, and selection criteria. In order to extract $A_{\rm FB}$ and $F_{\rm L}$, simultaneous fits are made to the $K^+\pi^-\mu^+\mu^-$ invariant mass distribution and the angular distributions. The partial branching fraction is measured by comparing the efficiency corrected yield of $B^0 \to K^{*0}\mu^+\mu^-$ decays to the yield of $B^0 \to J/\psi K^{*0}$, where $J/\psi \to \mu^+\mu^-$.

Candidate $B^0 \to K^{*0}\mu^+\mu^-$ events are first required to pass a hardware trigger which selects muons with a transverse momentum $p_{\rm T} > 1.48$ GeV/c. In the subsequent software trigger, at least one of the final state particles is required to have both $p_{\rm T} > 0.8$ GeV/c and impact parameter >100 μm with respect to all of the primary proton-proton interaction vertices in the event [4]. Finally, the tracks of two or more of the final state particles are required to form a vertex which is significantly displaced from the primary vertices in the event [5].

In the final event selection, candidates with $K^+\pi^-\mu^+\mu^-$ invariant mass in the range $5100 < m_{K^+\pi^-\mu^+\mu^-} < 5600$ MeV/c^2 and $K^+\pi^-$ invariant mass in the range $792 < m_{K^+\pi^-} < 992$ MeV/c^2 are accepted. Two types of backgrounds are then considered: combinatorial backgrounds, where the particles selected do not come from a single b-hadron decay, and peaking backgrounds, where a single decay is selected but with some of the particle types misidentified. In addition, the decays $B^0 \to J/\psi K^{*0}$ and $B^0 \to \psi(2S)K^{*0}$, where J/ψ, $\psi(2S) \to \mu^+\mu^-$, are removed by rejecting events with dimuon invariant mass $m_{\mu^+\mu^-}$ in the range $2946 < m_{\mu^+\mu^-} < 3176$ MeV/c^2 or $3586 < m_{\mu^+\mu^-} < 3776$ MeV/c^2.

The combinatorial background, which is smoothly distributed in the reconstructed $K^+\pi^-\mu^+\mu^-$ invariant mass, is reduced by using a boosted decision tree (BDT). The BDT uses information about the event kinematics, vertex and track quality, impact parameter, and particle identification information from the ring imaging Cherenkov and muon detectors. The variables that are used in the BDT are chosen so as to induce the minimum possible distortion in the angular and q^2 distributions. For example, no additional requirement is made on the $p_{\rm T}$ of both of the muons, as, at low q^2, this would remove a large proportion of events with $|\cos\theta_l| \sim 1$. The BDT is trained entirely on data, using samples that are independent of that which is used to make the measurements: Triggered and fully reconstructed $B^0 \to J/\psi K^{*0}$ events are used as a proxy for the signal decay, and events from the upper $B^0 \to K^{*0}\mu^+\mu^-$ mass sideband ($5350 < m_{K^+\pi^-\mu^+\mu^-} < 5600$ MeV/c^2) are used as a background sample. The lower mass sideband is not used, as it contains background events formed from partially reconstructed B decays. These events make a negligible contribution in the signal region and have properties different from the combinatorial background which is the dominant background in this region.

A cut is made on the BDT output in order to optimize the sensitivity to $A_{\rm FB}$ averaged over all q^2. The selected sample has a signal-to-background ratio of three to one.

Peaking backgrounds from $B_s^0 \to \phi\mu^+\mu^-$ (where $\phi \to K^+K^-$), $B^0 \to J/\psi K^{*0}$, and $B^0 \to \psi(2S)K^{*0}$ are considered and reduced with a set of vetoes. In each case, for the decay to be a potential signal candidate, at least one particle needs to be misidentified. For example, $B^0 \to J/\psi K^{*0}$ events where a kaon or pion is swapped for one of the muons peak around the nominal B^0 mass and evade the J/ψ veto described above. Vetoes for each of these backgrounds are formed by changing the relevant particle mass hypotheses and recomputing the invariant masses and by making use of the particle identification information. In order to avoid having a strongly peaking contribution to the $\cos\theta_K$ angular distribution in the upper mass sideband, $B^+ \to K^+\mu^+\mu^-$ candidates are removed. Events with $K^+\mu^+\mu^-$ invariant mass within 60 MeV/c^2 of the nominal B^+ mass are rejected. The vetoes for all of these peaking backgrounds remove a negligible amount of signal.

After the application of the BDT cut and the above vetoes, a fit is made to the $K^+\pi^-\mu^+\mu^-$ invariant mass distribution in the entire accepted mass range (see Fig. 1). A double-Gaussian distribution is used for the signal mass shape and an exponential function for the background. The signal shape is fixed from data using a fit to the $B^0 \to J/\psi K^{*0}$ mass peak. In the full q^2 range, in a signal mass window of ± 50 MeV/c^2 ($\pm 2.5\sigma$) around the measured B^0 mass, the fit gives an estimate of 337 ± 21 signal events with a background of 97 ± 6 events.

The residual peaking background is estimated by using simulated events. As detailed below, the accuracy of the

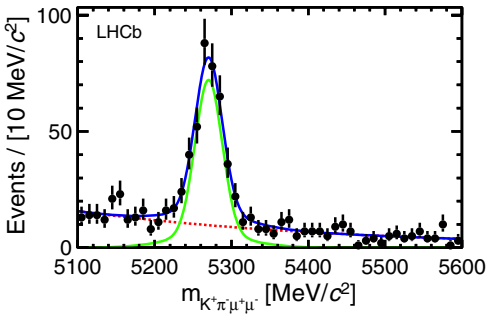

FIG. 1 (color online). $K^+\pi^-\mu^+\mu^-$ invariant mass distribution after the application of the full selection as data points with the fit overlaid. The signal component is the green (light) line, the background the red (dashed) line, and the full distribution the blue (dark) line.

simulation is verified by comparing the particle (mis)identification probabilities with those derived from control channels selected from the data. The residual peaking backgrounds are reduced to a level of 6.1 events, i.e., 1.8% of the 337 observed signal events. The backgrounds from $B_s^0 \to \phi\mu^+\mu^-$ and $B^0 \to J/\psi K^{*0}$ decays do not give rise to any forward-backward asymmetry and are ignored. However, in addition to the above backgrounds, $B^0 \to K^{*0}\mu^+\mu^-$ decays with the kaon and pion swapped give rise to a 0.7% contribution. The change in the sign of the particle which is taken to be the kaon results in a B^0 ($\bar{B}^0$) being reconstructed as a $\bar{B}^0$ (B^0), therefore changing the sign of $A_{\rm FB}$ for the candidate. This misidentification is accounted for in the fit for the angular observables.

The selected $B^0 \to K^{*0}\mu^+\mu^-$ candidates are weighted in order to correct for the effects of the reconstruction, trigger, and selection. The weights are derived from simulated $B^0 \to K^{*0}\mu^+\mu^-$ events and are normalized such that the average weight is 1. In order to be independent of the physics model used in the simulation, the weights are computed based on $\cos\theta_K$, $\cos\theta_l$, and q^2 on an event-by-event basis. The variation of detector efficiency with the ϕ angle is small, and ignoring this variation does not bias the measurements. Only events with $0.10 < q^2 < 19.00\ {\rm GeV}^2/c^4$ are analyzed.

Owing to the relatively unbiased selection, 89% of events have weights between 0.7 and 1.3, and only 3% of events have a weight above 2. The distortions in the distributions of $\cos\theta_K$, $\cos\theta_l$, and q^2 that are induced originate from two main sources. First, in order to pass through the iron muon filter and give hits in the muon stations, tracks must have at least 3 GeV/c momentum. At low q^2 this removes events with $|\cos\theta_l| \sim 1$. This effect stems from the geometry of the LHCb detector and is therefore relatively easy to model. Second, events with $\cos\theta_K \sim 1$, and hence a slow pion, are removed both by the pion reconstruction and by the impact parameter requirements used in the trigger and BDT selection.

A number of control samples are used to verify the simulation quality and to correct for differences with respect to the data. The reproduction of the B^0 momentum and pseudorapidity distributions is verified by using $B^0 \to J/\psi K^{*0}$ decays. These decays are also used to check that the simulation reproduces the measured properties of selected events. The hadron and muon (mis)identification probabilities are adjusted by using decays where the tested particle type can be determined without the use of the particle identification algorithms. A tag and probe approach with $J/\psi \to \mu^+\mu^-$ decays is used to isolate a clean sample of genuine muons. The decay $D^{*+} \to D^0\pi^+$, where $D^0 \to K^-\pi^+$, is used to give an unambiguous source of kaons and pions. The statistical precision with which it is possible to make the data-simulation comparison gives rise to a systematic uncertainty in the weights which is evaluated below.

The observables $A_{\rm FB}$ and $F_{\rm L}$ are extracted in bins of q^2. In each bin, a simultaneous fit to the $K^+\pi^-\mu^+\mu^-$ invariant mass distribution and the $\cos\theta_K$ and $\cos\theta_l$ distributions is performed. The angular distributions are fitted both in the signal mass window and in the upper mass sideband which determines the background parameters. The angular distributions for the signal are given by Eqs. (1) and (2), and a second-order polynomial in $\cos\theta_K$ and in $\cos\theta_l$ is used for the background.

In order to obtain a positive probability density function over the entire angular range, Eqs. (1) and (2) imply that the conditions $|A_{\rm FB}| \leq \frac{3}{4}(1 - F_{\rm L})$ and $0 < F_{\rm L} < 1$ must be satisfied. To account for this, the maximum likelihood values for $A_{\rm FB}$ and $F_{\rm L}$ are extracted by performing a profile-likelihood scan over the allowed range. The uncertainty on the central value of $A_{\rm FB}$ and $F_{\rm L}$ is calculated by integrating the probability density extracted from the likelihood, assuming a flat prior in $A_{\rm FB}$ and $F_{\rm L}$, inside the allowed range. This gives an (asymmetric) 68% confidence interval.

The partial branching fraction is measured in each of the q^2 bins from a fit to the efficiency corrected $K^+\pi^-\mu^+\mu^-$ mass spectrum. The efficiencies are determined relative to the $B^0 \to J/\psi K^{*0}$ decay which is used as a normalization mode.

The event weighting and fitting procedure is validated by fitting the angular distribution of $B^0 \to J/\psi K^{*0}$ events, where the physics parameters are known from previous measurements [6]. The product of the $B^0 \to J/\psi K^{*0}$ and $J/\psi \to \mu^+\mu^-$ branching fractions is ~75 times larger than the branching fraction of $B^0 \to K^{*0}\mu^+\mu^-$, allowing a precise test of the procedure to be made. Fitting the $B^0 \to J/\psi K^{*0}$ angular distribution, weighted according to the event-by-event procedure described above, yields values for $F_{\rm L}$ and $A_{\rm FB}$ in good agreement with those found previously.

For $B^0 \to K^{*0}\mu^+\mu^-$, the fit results for $A_{\rm FB}$, $F_{\rm L}$, and $d\mathcal{B}/dq^2$ are shown in Fig. 2 and are tabulated together with the signal and background yields in Table I. The fit projections are available online [7]. Signal candidates are observed in each q^2 bin with more than 5σ significance. The compatibility of the fits and the data are assessed by using a binned χ^2 test, and all fits are found to be of good quality. The measurements in all three quantities are more precise than those of previous experiments and are in good agreement with the SM predictions. The predictions are taken from Ref. [8]. In the low q^2 region, they rely on the factorization approach [9], which loses accuracy when approaching the J/ψ resonance; in the high q^2 region, an operator product expansion in the inverse b-quark mass, $1/m_b$, and in $1/\sqrt{q^2}$ is used [10], which is valid only above the open charm threshold. In both regions the form factor calculations are taken from Ref. [11], and a dimensional estimate is made on the uncertainty from expansion corrections [12].

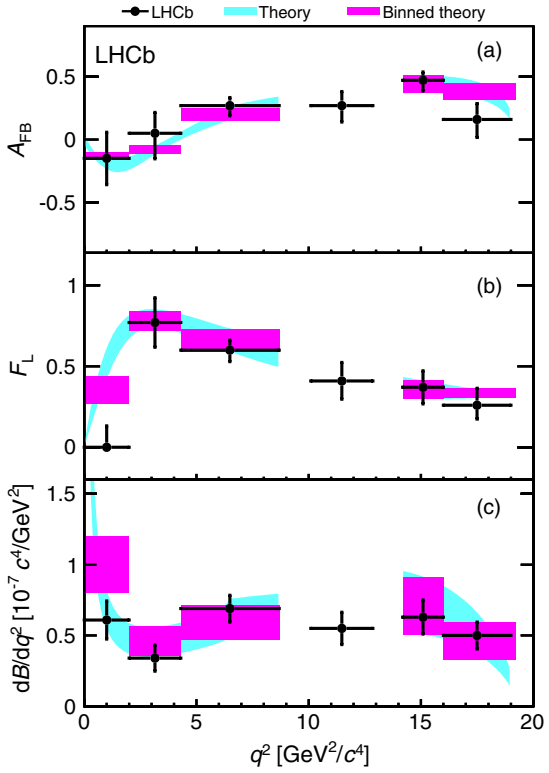

FIG. 2 (color online). A_{FB} (a), F_L (b), and $d\mathcal{B}/dq^2$ (c) as a function of q^2. The SM prediction is given by the cyan (light) band, and this prediction rate-averaged across the q^2 bins is indicated by the purple (dark) regions. No SM prediction is shown for the region between the two regimes in which the theoretical calculations are made (see the text).

In the $1.00 < q^2 < 6.00$ GeV$^2/c^4$ region, the fit gives $A_{FB} = -0.06^{+0.13}_{-0.14} \pm 0.04$, $F_L = 0.55 \pm 0.10 \pm 0.03$, and $d\mathcal{B}/dq^2 = (0.42 \pm 0.06 \pm 0.03) \times 10^{-7}$ c^4/GeV^2, where the first error is statistical and the second systematic. The theoretical predictions in the same q^2 range are $A_{FB} = -0.04 \pm 0.03$, $F_L = 0.74^{+0.06}_{-0.07}$, and $d\mathcal{B}/dq^2 = (0.50^{+0.11}_{-0.10}) \times 10^{-7}$ c^4/GeV^2. The LHCb A_{FB} measurement is a factor of 1.5–2.0 more precise than previous measurements from the Belle, CDF, and *BABAR* Collaborations [2] which are, respectively, $A_{FB} = 0.26^{+0.27}_{-0.30} \pm 0.07$, $A_{FB} = 0.29^{+0.20}_{-0.23} \pm 0.07$, and, for $q^2 < 6.25$ GeV$^2/c^4$, $A_{FB} = 0.24^{+0.18}_{-0.23} \pm 0.05$. The positive value of A_{FB} preferred in the $1.00 < q^2 < 6.00$ GeV$^2/c^4$ range in these previous measurements is not favored by the LHCb data. The previous measurements of F_L in the same q^2 regions are $F_L = 0.67 \pm 0.23 \pm 0.05$ (Belle), $F_L = 0.69^{+0.19}_{-0.21} \pm 0.08$ (CDF), and $F_L = 0.35 \pm 0.16 \pm 0.04$ (*BABAR*). These are in good agreement with the LHCb result.

For the determination of A_{FB} and F_L, the dominant systematic uncertainties arise from the event-by-event weights which are extracted from simulated events and from the model used to describe the angular distribution of the background. The uncertainty on the event-by-event weights is evaluated by fluctuating these weights within their statistical uncertainties and repeating the fitting procedure. The uncertainty from the background model which is used is estimated by changing this model to one which uses binned templates from the upper mass sideband rather than a polynomial parameterization.

The dominant systematic errors for the determination of $d\mathcal{B}/dq^2$ arise from the uncertainties on the particle identification and track reconstruction efficiencies. These efficiencies are extracted from control channels and are limited by the relevant sample sizes. The systematic uncertainty is estimated by fluctuating the efficiencies within the relevant uncertainties and repeating the fitting procedure. An additional systematic uncertainty of ~4% arises from the uncertainty in the $B^0 \to J/\psi K^{*0}$ and $J/\psi \to \mu^+\mu^-$ branching fractions [13].

The total systematic error on each of A_{FB} and F_L ($d\mathcal{B}/dq^2$) is typically ~30% (50%) of the statistical error and, hence, adds ~4% (~ 11%) to the total uncertainty.

In summary, by using 0.37 fb^{-1} of data taken with the LHCb detector during 2011, A_{FB}, F_L, and $d\mathcal{B}/dq^2$ have been determined for the decay $B^0 \to K^{*0}\mu^+\mu^-$. These are the most precise measurements of these quantities to date.

TABLE I. Central values with statistical and systematic uncertainties for A_{FB}, F_L, and $d\mathcal{B}/dq^2$ as a function of q^2. The $B^0 \to K^{*0}\mu^+\mu^-$ signal and background yields in the ± 50 MeV$/c^2$ signal mass window with their statistical uncertainties are also indicated, together with the statistical significance of the signal peak that is observed. The significance is computed from the change in the likelihood, fitting with and without the signal component to the mass shape. In the case with the signal component, the signal shape is fixed from data using a fit to the $B^0 \to J/\psi K^{*0}$ mass peak.

q^2 (GeV$^2/c^4$)	A_{FB}	F_L	$d\mathcal{B}/dq^2$ ($\times 10^{-7}$ c^4/GeV^2)	Signal yield	Background yield	Significance (σ)
$0.10 < q^2 < 2.00$	$-0.15 \pm 0.20 \pm 0.06$	$0.00^{+0.13}_{-0.00} \pm 0.02$	$0.61 \pm 0.12 \pm 0.06$	48.6 ± 8.1	16.2 ± 2.3	8.6
$2.00 < q^2 < 4.30$	$0.05^{+0.16}_{-0.20} \pm 0.04$	$0.77 \pm 0.15 \pm 0.03$	$0.34 \pm 0.09 \pm 0.02$	26.5 ± 6.5	15.7 ± 2.2	5.4
$4.30 < q^2 < 8.68$	$0.27^{+0.06}_{-0.08} \pm 0.02$	$0.60^{+0.06}_{-0.07} \pm 0.01$	$0.69 \pm 0.08 \pm 0.05$	104.7 ± 11.9	31.7 ± 3.3	12.4
$10.09 < q^2 < 12.86$	$0.27^{+0.11}_{-0.13} \pm 0.02$	$0.41 \pm 0.11 \pm 0.03$	$0.55 \pm 0.09 \pm 0.07$	62.2 ± 9.2	20.4 ± 2.6	9.6
$14.18 < q^2 < 16.00$	$0.47^{+0.06}_{-0.08} \pm 0.03$	$0.37 \pm 0.09 \pm 0.05$	$0.63 \pm 0.11 \pm 0.05$	44.2 ± 7.0	4.2 ± 1.3	10.2
$16.00 < q^2 < 19.00$	$0.16^{+0.11}_{-0.13} \pm 0.06$	$0.26^{+0.10}_{-0.08} \pm 0.03$	$0.50 \pm 0.08 \pm 0.05$	53.4 ± 8.1	7.0 ± 1.7	9.8
$1.00 < q^2 < 6.00$	$-0.06^{+0.13}_{-0.14} \pm 0.04$	$0.55 \pm 0.10 \pm 0.03$	$0.42 \pm 0.06 \pm 0.03$	76.5 ± 10.6	33.1 ± 3.2	9.9

All three observables show good agreement with the SM predictions.

We express our gratitude to our colleagues in the CERN accelerator departments for the excellent performance of the LHC. We thank the technical and administrative staff at CERN and at the LHCb institutes and acknowledge support from the National Agencies: CAPES, CNPq, FAPERJ, and FINEP (Brazil); CERN; NSFC (China); CNRS/IN2P3 (France); BMBF, DFG, HGF, and MPG (Germany); SFI (Ireland); INFN (Italy); FOM and NWO (The Netherlands); SCSR (Poland); ANCS (Romania); MinES of Russia and Rosatom (Russia); MICINN, XuntaGal, and GENCAT (Spain); SNSF and SER (Switzerland); NAS Ukraine (Ukraine); STFC (United Kingdom); NSF (USA). We also acknowledge the support received from the ERC under FP7 and the Region Auvergne.

[1] F. Krüger, L. M. Sehgal, N. Sinha, and R. Sinha, Phys. Rev. D **61**, 114028 (2000).

[2] B. Aubert *et al.* (*BABAR* Collaboration), Phys. Rev. D **79**, 031102 (2009); J.-T. Wei *et al.* (Belle Collaboration), Phys. Rev. Lett. **103**, 171801 (2009); T. Aaltonen *et al.* (CDF Collaboration), arXiv:1108.0695.

[3] A. A. Alves, Jr. *et al.* (LHCb Collaboration), JINST **3**, S08005 (2008).

[4] V. V. Gligorov, Report No. LHCb-PUB-2011-003.

[5] M. Williams *et al.*, Report No. LHCb-PUB-2011-002.

[6] B. Aubert *et al.* (*BABAR* Collaboration), Phys. Rev. D **76**, 031102 (2007).

[7] See Supplemental Material at http://link.aps.org/supplemental/10.1103/PhysRevLett.108.181806 for the $\cos\theta_l$, $\cos\theta_K$, and $K^+\pi^-\mu^+\mu^-$ invariant mass distributions with the fit superimposed.

[8] C. Bobeth, G. Hiller, and D. van Dyk, J. High Energy Phys. 07 (2011) 067.

[9] M. Beneke, T. Feldmann, and D. Seidel, Nucl. Phys. **B612**, 25 (2001).

[10] B. Grinstein and D. Pirjol, Phys. Rev. D **70**, 114005 (2004).

[11] P. Ball and R. Zwicky, Phys. Rev. D **71**, 014029 (2005).

[12] U. Egede, T. Hurth, J. Matias, M. Ramon, and W. Reece, J. High Energy Phys. 11 (2008) 032.

[13] K. Nakamura *et al.* (Particle Data Group), J. Phys. G **37**, 075021 (2010).

R. Aaij,[23] C. Abellan Beteta,[35,n] B. Adeva,[36] M. Adinolfi,[42] C. Adrover,[6] A. Affolder,[48] Z. Ajaltouni,[5] J. Albrecht,[37] F. Alessio,[37] M. Alexander,[47] G. Alkhazov,[29] P. Alvarez Cartelle,[36] A. A. Alves, Jr.,[22] S. Amato,[2] Y. Amhis,[38] J. Anderson,[39] R. B. Appleby,[50] O. Aquines Gutierrez,[10] F. Archilli,[18,37] L. Arrabito,[53] A. Artamonov,[34] M. Artuso,[52,37] E. Aslanides,[6] G. Auriemma,[22,m] S. Bachmann,[11] J. J. Back,[44] D. S. Bailey,[50] V. Balagura,[30,37] W. Baldini,[16] R. J. Barlow,[50] C. Barschel,[37] S. Barsuk,[7] W. Barter,[43] A. Bates,[47] C. Bauer,[10] Th. Bauer,[23] A. Bay,[38] I. Bediaga,[1] S. Belogurov,[30] K. Belous,[34] I. Belyaev,[30,37] E. Ben-Haim,[8] M. Benayoun,[8] G. Bencivenni,[18] S. Benson,[46] J. Benton,[42] R. Bernet,[39] M.-O. Bettler,[17] M. van Beuzekom,[23] A. Bien,[11] S. Bifani,[12] T. Bird,[50] A. Bizzeti,[17,h] P. M. Bjørnstad,[50] T. Blake,[37] F. Blanc,[38] C. Blanks,[49] J. Blouw,[11] S. Blusk,[52] A. Bobrov,[33] V. Bocci,[22] A. Bondar,[33] N. Bondar,[29] W. Bonivento,[15] S. Borghi,[47,50] A. Borgia,[52] T. J. V. Bowcock,[48] C. Bozzi,[16] T. Brambach,[9] J. van den Brand,[24] J. Bressieux,[38] D. Brett,[50] M. Britsch,[10] T. Britton,[52] N. H. Brook,[42] H. Brown,[48] A. Büchler-Germann,[39] I. Burducea,[28] A. Bursche,[39] J. Buytaert,[37] S. Cadeddu,[15] O. Callot,[7] M. Calvi,[20,j] M. Calvo Gomez,[35,n] A. Camboni,[35] P. Campana,[18,37] A. Carbone,[14] G. Carboni,[21,k] R. Cardinale,[19,37,i] A. Cardini,[15] L. Carson,[49] K. Carvalho Akiba,[2] G. Casse,[48] M. Cattaneo,[37] Ch. Cauet,[9] M. Charles,[51] Ph. Charpentier,[37] N. Chiapolini,[39] K. Ciba,[37] X. Cid Vidal,[36] G. Ciezarek,[49] P. E. L. Clarke,[46,37] M. Clemencic,[37] H. V. Cliff,[43] J. Closier,[37] C. Coca,[28] V. Coco,[23] J. Cogan,[6] P. Collins,[37] A. Comerma-Montells,[35] F. Constantin,[28] A. Contu,[51] A. Cook,[42] M. Coombes,[42] G. Corti,[37] G. A. Cowan,[38] R. Currie,[46] C. D'Ambrosio,[37] P. David,[8] P. N. Y. David,[23] I. De Bonis,[4] S. De Capua,[21,k] M. De Cian,[39] F. De Lorenzi,[12] J. M. De Miranda,[1] L. De Paula,[2] P. De Simone,[18] D. Decamp,[4] M. Deckenhoff,[9] H. Degaudenzi,[38,37] L. Del Buono,[8] C. Deplano,[15] D. Derkach,[14,37] O. Deschamps,[5] F. Dettori,[24] J. Dickens,[43] H. Dijkstra,[37] P. Diniz Batista,[1] F. Domingo Bonal,[35,n] S. Donleavy,[48] F. Dordei,[11] A. Dosil Suárez,[36] D. Dossett,[44] A. Dovbnya,[40] F. Dupertuis,[38] R. Dzhelyadin,[34] A. Dziurda,[25] S. Easo,[45] U. Egede,[49] V. Egorychev,[30] S. Eidelman,[33] D. van Eijk,[23] F. Eisele,[11] S. Eisenhardt,[46] R. Ekelhof,[9] L. Eklund,[47] Ch. Elsasser,[39] D. Elsby,[55] D. Esperante Pereira,[36] L. Estève,[43] A. Falabella,[16,14,e] E. Fanchini,[20,j] C. Färber,[11] G. Fardell,[46] C. Farinelli,[23] S. Farry,[12] V. Fave,[38] V. Fernandez Albor,[36] M. Ferro-Luzzi,[37] S. Filippov,[32] C. Fitzpatrick,[46] M. Fontana,[10] F. Fontanelli,[19,i] R. Forty,[37] M. Frank,[37] C. Frei,[37] M. Frosini,[17,37,f] S. Furcas,[20] A. Gallas Torreira,[36] D. Galli,[14,c] M. Gandelman,[2] P. Gandini,[51] Y. Gao,[3] J-C. Garnier,[37] J. Garofoli,[52] J. Garra Tico,[43] L. Garrido,[35] D. Gascon,[35] C. Gaspar,[37] N. Gauvin,[38] M. Gersabeck,[37] T. Gershon,[44,37] Ph. Ghez,[4] V. Gibson,[43] V. V. Gligorov,[37] C. Göbel,[54] D. Golubkov,[30] A. Golutvin,[49,30,37] A. Gomes,[2] H. Gordon,[51] M. Grabalosa Gándara,[35] R. Graciani Diaz,[35] L. A. Granado Cardoso,[37] E. Graugés,[35] G. Graziani,[17] A. Grecu,[28] E. Greening,[51] S. Gregson,[43] B. Gui,[52] E. Gushchin,[32] Yu. Guz,[34] T. Gys,[37] G. Haefeli,[38] C. Haen,[37] S. C. Haines,[43] T. Hampson,[42]

S. Hansmann-Menzemer,[11] R. Harji,[49] N. Harnew,[51] J. Harrison,[50] P. F. Harrison,[44] T. Hartmann,[56] J. He,[7] V. Heijne,[23] K. Hennessy,[48] P. Henrard,[5] J. A. Hernando Morata,[36] E. van Herwijnen,[37] E. Hicks,[48] K. Holubyev,[11] P. Hopchev,[4] W. Hulsbergen,[23] P. Hunt,[51] T. Huse,[48] R. S. Huston,[12] D. Hutchcroft,[48] D. Hynds,[47] V. Iakovenko,[41] P. Ilten,[12] J. Imong,[42] R. Jacobsson,[37] A. Jaeger,[11] M. Jahjah Hussein,[5] E. Jans,[23] F. Jansen,[23] P. Jaton,[38] B. Jean-Marie,[7] F. Jing,[3] M. John,[51] D. Johnson,[51] C. R. Jones,[43] B. Jost,[37] M. Kaballo,[9] S. Kandybei,[40] M. Karacson,[37] T. M. Karbach,[9] J. Keaveney,[12] I. R. Kenyon,[55] U. Kerzel,[37] T. Ketel,[24] A. Keune,[38] B. Khanji,[6] Y. M. Kim,[46] M. Knecht,[38] P. Koppenburg,[23] A. Kozlinskiy,[23] L. Kravchuk,[32] K. Kreplin,[11] M. Kreps,[44] G. Krocker,[11] P. Krokovny,[11] F. Kruse,[9] K. Kruzelecki,[37] M. Kucharczyk,[20,25,37,j] T. Kvaratskheliya,[30,37] V. N. La Thi,[38] D. Lacarrere,[37] G. Lafferty,[50] A. Lai,[15] D. Lambert,[46] R. W. Lambert,[24] E. Lanciotti,[37] G. Lanfranchi,[18] C. Langenbruch,[11] T. Latham,[44] C. Lazzeroni,[55] R. Le Gac,[6] J. van Leerdam,[23] J.-P. Lees,[4] R. Lefèvre,[5] A. Leflat,[31,37] J. Lefrançois,[7] O. Leroy,[6] T. Lesiak,[25] L. Li,[3] L. Li Gioi,[5] M. Lieng,[9] M. Liles,[48] R. Lindner,[37] C. Linn,[11] B. Liu,[3] G. Liu,[37] J. von Loeben,[20] J. H. Lopes,[2] E. Lopez Asamar,[35] N. Lopez-March,[38] H. Lu,[38,3] J. Luisier,[38] A. Mac Raighne,[47] F. Machefert,[7] I. V. Machikhiliyan,[4,30] F. Maciuc,[10] O. Maev,[29,37] J. Magnin,[1] S. Malde,[51] R. M. D. Mamunur,[37] G. Manca,[15,d] G. Mancinelli,[6] N. Mangiafave,[43] U. Marconi,[14] R. Märki,[38] J. Marks,[11] G. Martellotti,[22] A. Martens,[8] L. Martin,[51] A. Martín Sánchez,[7] D. Martinez Santos,[37] A. Massafferri,[1] Z. Mathe,[12] C. Matteuzzi,[20] M. Matveev,[29] E. Maurice,[6] B. Maynard,[52] A. Mazurov,[16,32,37] G. McGregor,[50] R. McNulty,[12] M. Meissner,[11] M. Merk,[23] J. Merkel,[9] R. Messi,[21,k] S. Miglioranzi,[37] D. A. Milanes,[13,37] M.-N. Minard,[4] J. Molina Rodriguez,[54] S. Monteil,[5] D. Moran,[12] P. Morawski,[25] R. Mountain,[52] I. Mous,[23] F. Muheim,[46] K. Müller,[39] R. Muresan,[28,38] B. Muryn,[26] B. Muster,[38] M. Musy,[35] J. Mylroie-Smith,[48] P. Naik,[42] T. Nakada,[38] R. Nandakumar,[45] I. Nasteva,[1] M. Nedos,[9] M. Needham,[46] N. Neufeld,[37] C. Nguyen-Mau,[38,o] M. Nicol,[7] V. Niess,[5] N. Nikitin,[31] A. Nomerotski,[51] A. Novoselov,[34] A. Oblakowska-Mucha,[26] V. Obraztsov,[34] S. Oggero,[23] S. Ogilvy,[47] O. Okhrimenko,[41] R. Oldeman,[15,d] M. Orlandea,[28] J. M. Otalora Goicochea,[2] P. Owen,[49] K. Pal,[52] J. Palacios,[39] A. Palano,[13,b] M. Palutan,[18] J. Panman,[37] A. Papanestis,[45] M. Pappagallo,[47] C. Parkes,[50,37] C. J. Parkinson,[49] G. Passaleva,[17] G. D. Patel,[48] M. Patel,[49] S. K. Paterson,[49] G. N. Patrick,[45] C. Patrignani,[19,i] C. Pavel-Nicorescu,[28] A. Pazos Alvarez,[36] A. Pellegrino,[23] G. Penso,[22,l] M. Pepe Altarelli,[37] S. Perazzini,[14,c] D. L. Perego,[20,j] E. Perez Trigo,[36] A. Pérez-Calero Yzquierdo,[35] P. Perret,[5] M. Perrin-Terrin,[6] G. Pessina,[20] A. Petrella,[16,37] A. Petrolini,[19,i] A. Phan,[52] E. Picatoste Olloqui,[35] B. Pie Valls,[35] B. Pietrzyk,[4] T. Pilař,[44] D. Pinci,[22] R. Plackett,[47] S. Playfer,[46] M. Plo Casasus,[36] G. Polok,[25] A. Poluektov,[44,33] E. Polycarpo,[2] D. Popov,[10] B. Popovici,[28] C. Potterat,[35] A. Powell,[51] J. Prisciandaro,[38] V. Pugatch,[41] A. Puig Navarro,[35] W. Qian,[52] J. H. Rademacker,[42] B. Rakotomiaramanana,[38] M. S. Rangel,[2] I. Raniuk,[40] G. Raven,[24] S. Redford,[51] M. M. Reid,[44] A. C. dos Reis,[1] S. Ricciardi,[45] K. Rinnert,[48] D. A. Roa Romero,[5] P. Robbe,[7] E. Rodrigues,[47,50] F. Rodrigues,[2] P. Rodriguez Perez,[36] G. J. Rogers,[43] S. Roiser,[37] V. Romanovsky,[34] M. Rosello,[35,n] J. Rouvinet,[38] T. Ruf,[37] H. Ruiz,[35] G. Sabatino,[21,k] J. J. Saborido Silva,[36] N. Sagidova,[29] P. Sail,[47] B. Saitta,[15,d] C. Salzmann,[39] M. Sannino,[19,i] R. Santacesaria,[22] C. Santamarina Rios,[36] R. Santinelli,[37] E. Santovetti,[21,k] M. Sapunov,[6] A. Sarti,[18,l] C. Satriano,[22,m] A. Satta,[21] M. Savrie,[16,e] D. Savrina,[30] P. Schaack,[49] M. Schiller,[24] S. Schleich,[9] M. Schlupp,[9] M. Schmelling,[10] B. Schmidt,[37] O. Schneider,[38] A. Schopper,[37] M.-H. Schune,[7] R. Schwemmer,[37] B. Sciascia,[18] A. Sciubba,[18,l] M. Seco,[36] A. Semennikov,[30] K. Senderowska,[26] I. Sepp,[49] N. Serra,[39] J. Serrano,[6] P. Seyfert,[11] M. Shapkin,[34] I. Shapoval,[40,37] P. Shatalov,[30] Y. Shcheglov,[29] T. Shears,[48] L. Shekhtman,[33] O. Shevchenko,[40] V. Shevchenko,[30] R. Silva Coutinho,[44] A. Shires,[49] T. Skwarnicki,[52] A. C. Smith,[37] N. A. Smith,[48] E. Smith,[51,45] K. Sobczak,[5] F. J. P. Soler,[47] A. Solomin,[42] F. Soomro,[18] B. Souza De Paula,[2] B. Spaan,[9] A. Sparkes,[46] P. Spradlin,[47] F. Stagni,[37] S. Stahl,[11] O. Steinkamp,[39] S. Stoica,[28] S. Stone,[52,37] B. Storaci,[23] M. Straticiuc,[28] U. Straumann,[39] V. K. Subbiah,[37] S. Swientek,[9] M. Szczekowski,[27] P. Szczypka,[38] T. Szumlak,[26] S. T'Jampens,[4] E. Teodorescu,[28] F. Teubert,[37] C. Thomas,[51] E. Thomas,[37] J. van Tilburg,[11] V. Tisserand,[4] M. Tobin,[39] S. Topp-Joergensen,[51] N. Torr,[51] E. Tournefier,[4,49] M. T. Tran,[38] A. Tsaregorodtsev,[6] N. Tuning,[23] M. Ubeda Garcia,[37] A. Ukleja,[27] P. Urquijo,[52] U. Uwer,[11] V. Vagnoni,[14] G. Valenti,[14] R. Vazquez Gomez,[35] P. Vazquez Regueiro,[36] S. Vecchi,[16] J. J. Velthuis,[42] M. Veltri,[17,g] B. Viaud,[7] I. Videau,[7] X. Vilasis-Cardona,[35,n] J. Visniakov,[36] A. Vollhardt,[39] D. Volyanskyy,[10] D. Voong,[42] A. Vorobyev,[29] H. Voss,[10] S. Wandernoth,[11] J. Wang,[52] D. R. Ward,[43] N. K. Watson,[55] A. D. Webber,[50] D. Websdale,[49] M. Whitehead,[44] D. Wiedner,[11] L. Wiggers,[23] G. Wilkinson,[51] M. P. Williams,[44,45] M. Williams,[49] F. F. Wilson,[45] J. Wishahi,[9] M. Witek,[25] W. Witzeling,[37] S. A. Wotton,[43] K. Wyllie,[37] Y. Xie,[46] F. Xing,[51] Z. Xing,[52] Z. Yang,[3] R. Young,[46] O. Yushchenko,[34] M. Zavertyaev,[10,a] F. Zhang,[3] L. Zhang,[52] W. C. Zhang,[12] Y. Zhang,[3] A. Zhelezov,[11] L. Zhong,[3] E. Zverev,[31] and A. Zvyagin[37]

(LHCb Collaboration)

[1]*Centro Brasileiro de Pesquisas Físicas (CBPF), Rio de Janeiro, Brazil*
[2]*Universidade Federal do Rio de Janeiro (UFRJ), Rio de Janeiro, Brazil*
[3]*Center for High Energy Physics, Tsinghua University, Beijing, China*
[4]*LAPP, Université de Savoie, CNRS/IN2P3, Annecy-Le-Vieux, France*
[5]*Clermont Université, Université Blaise Pascal, CNRS/IN2P3, LPC, Clermont-Ferrand, France*
[6]*CPPM, Aix-Marseille Université, CNRS/IN2P3, Marseille, France*
[7]*LAL, Université Paris-Sud, CNRS/IN2P3, Orsay, France*
[8]*LPNHE, Université Pierre et Marie Curie, Université Paris Diderot, CNRS/IN2P3, Paris, France*
[9]*Fakultät Physik, Technische Universität Dortmund, Dortmund, Germany*
[10]*Max-Planck-Institut für Kernphysik (MPIK), Heidelberg, Germany*
[11]*Physikalisches Institut, Ruprecht-Karls-Universität Heidelberg, Heidelberg, Germany*
[12]*School of Physics, University College Dublin, Dublin, Ireland*
[13]*Sezione INFN di Bari, Bari, Italy*
[14]*Sezione INFN di Bologna, Bologna, Italy*
[15]*Sezione INFN di Cagliari, Cagliari, Italy*
[16]*Sezione INFN di Ferrara, Ferrara, Italy*
[17]*Sezione INFN di Firenze, Firenze, Italy*
[18]*Laboratori Nazionali dell'INFN di Frascati, Frascati, Italy*
[19]*Sezione INFN di Genova, Genova, Italy*
[20]*Sezione INFN di Milano Bicocca, Milano, Italy*
[21]*Sezione INFN di Roma Tor Vergata, Roma, Italy*
[22]*Sezione INFN di Roma La Sapienza, Roma, Italy*
[23]*Nikhef National Institute for Subatomic Physics, Amsterdam, The Netherlands*
[24]*Nikhef National Institute for Subatomic Physics and Vrije Universiteit, Amsterdam, The Netherlands*
[25]*Henryk Niewodniczanski Institute of Nuclear Physics Polish Academy of Sciences, Kraców, Poland*
[26]*AGH University of Science and Technology, Kraców, Poland*
[27]*Soltan Institute for Nuclear Studies, Warsaw, Poland*
[28]*Horia Hulubei National Institute of Physics and Nuclear Engineering, Bucharest-Magurele, Romania*
[29]*Petersburg Nuclear Physics Institute (PNPI), Gatchina, Russia*
[30]*Institute of Theoretical and Experimental Physics (ITEP), Moscow, Russia*
[31]*Institute of Nuclear Physics, Moscow State University (SINP MSU), Moscow, Russia*
[32]*Institute for Nuclear Research of the Russian Academy of Sciences (INR RAN), Moscow, Russia*
[33]*Budker Institute of Nuclear Physics (SB RAS) and Novosibirsk State University, Novosibirsk, Russia*
[34]*Institute for High Energy Physics (IHEP), Protvino, Russia*
[35]*Universitat de Barcelona, Barcelona, Spain*
[36]*Universidad de Santiago de Compostela, Santiago de Compostela, Spain*
[37]*European Organization for Nuclear Research (CERN), Geneva, Switzerland*
[38]*Ecole Polytechnique Fédérale de Lausanne (EPFL), Lausanne, Switzerland*
[39]*Physik-Institut, Universität Zürich, Zürich, Switzerland*
[40]*NSC Kharkiv Institute of Physics and Technology (NSC KIPT), Kharkiv, Ukraine*
[41]*Institute for Nuclear Research of the National Academy of Sciences (KINR), Kyiv, Ukraine*
[42]*H. H. Wills Physics Laboratory, University of Bristol, Bristol, United Kingdom*
[43]*Cavendish Laboratory, University of Cambridge, Cambridge, United Kingdom*
[44]*Department of Physics, University of Warwick, Coventry, United Kingdom*
[45]*STFC Rutherford Appleton Laboratory, Didcot, United Kingdom*
[46]*School of Physics and Astronomy, University of Edinburgh, Edinburgh, United Kingdom*
[47]*School of Physics and Astronomy, University of Glasgow, Glasgow, United Kingdom*
[48]*Oliver Lodge Laboratory, University of Liverpool, Liverpool, United Kingdom*
[49]*Imperial College London, London, United Kingdom*
[50]*School of Physics and Astronomy, University of Manchester, Manchester, United Kingdom*
[51]*Department of Physics, University of Oxford, Oxford, United Kingdom*
[52]*Syracuse University, Syracuse, New York, USA*
[53]*CC-IN2P3, CNRS/IN2P3, Lyon-Villeurbanne, France, associated member*
[54]*Pontifícia Universidade Católica do Rio de Janeiro (PUC-Rio), Rio de Janeiro, Brazil, associated to Universidade Federal do Rio de Janeiro (UFRJ), Rio de Janeiro, Brazil*
[55]*University of Birmingham, Birmingham, United Kingdom*

[56]*Physikalisches Institut, Universität Rostock, Rostock, Germany, associated to Physikalisches Institut, Ruprecht-Karls-Universität Heidelberg, Heidelberg, Germany*

[a]Also at P. N. Lebedev Physical Institute, Russian Academy of Science (LPI RAS), Moscow, Russia.
[b]Also at Università di Bari, Bari, Italy.
[c]Also at Università di Bologna, Bologna, Italy.
[d]Also at Università di Cagliari, Cagliari, Italy.
[e]Also at Università di Ferrara, Ferrara, Italy.
[f]Also at Università di Firenze, Firenze, Italy.
[g]Also at Università di Urbino, Urbino, Italy.
[h]Also at Università di Modena e Reggio Emilia, Modena, Italy.
[i]Also at Università di Genova, Genova, Italy.
[j]Also at Università di Milano Bicocca, Milano, Italy.
[k]Also at Università di Roma Tor Vergata, Roma, Italy.
[l]Also at Università di Roma La Sapienza, Roma, Italy.
[m]Also at Università della Basilicata, Potenza, Italy.
[n]Also at LIFAELS, La Salle, Universitat Ramon Llull, Barcelona, Spain.
[o]Also at Hanoi University of Science, Hanoi, Vietnam.